

Hemocyte-Mediated Shell Mineralization in the Eastern Oyster

Andrew S. Mount,^{1*} A. P. Wheeler,¹
Rajesh P. Paradkar,^{2†} D. Snider³

The growth of molluscan shell crystals is usually thought to be initiated from solution by extracellular organic matrix. We report a class of granulocytic hemocytes that may be directly involved in shell crystal production for oysters. On the basis of scanning electron microscopy (SEM) and x-ray microanalysis, these granulocytes contain calcium carbonate crystals, and they increase in abundance relative to other hemocytes following experimentally induced shell regeneration. Hemocytes are observed at the mineralization front using vital fluorescent staining and SEM. Some cells are observed releasing crystals that are subsequently remodeled, thereby at least augmenting matrix-mediated crystal-forming processes in this system.

Molluscan shell formation is often cited as resulting in large measure from extracellular events mediated by organic matrix secreted from the mantle epithelium (1–3). The matrix-mediated hypothesis states that the complex organic matrix induces heterogeneous nucleation of calcium carbonate crystals on its surface and regulates crystal growth, thereby forming the crystal morphologies that are unique to the various layers of molluscan shell. In vitro studies using natural and synthetic molecular systems have shown that matrix control of crystal morphology is possible (3–10). However, these experiments are often conducted at levels of calcium carbonate supersaturation that are far higher than values reported for the extracellular environment in which shell is formed, leaving the extent of matrix involvement in crystal induction an open question. When in vitro experiments were conducted using insoluble matrix extracts (IM) from the shell of the oyster *Crassostrea virginica*, the level of supersaturation required to induce mineralization was no lower than that of controls (11). Furthermore, analysis using flow-cell atomic-force microscopy of oyster shell foliated pieces revealed that in situ matrix-coated crystals do not induce secondary nucleation events on their surfaces (12).

One alternative to the matrix-mediated hypothesis is that crystal nucleation is intracellular and that crystallogenic cells supply

nascent crystals to the mineralization front. Earlier radioisotope analyses of calcium uptake in the oyster support this hypothesis. These studies have shown that only 2.4% of the calcium of the shell-forming mantle turns over rapidly (13–15), revealing a large, nonexchangeable pool of calcium sequestered in these tissues. Although the source of the nonexchangeable pool has not been identified, one candidate is the circulating amoeboid hemocytes. These cells can migrate to the surface of the shell-facing outer mantle epithelium (OME) (16, 17), and one class of the hemocytes contains granules that are birefringent when examined by polarized light microscopy. We reasoned that some of these granules might be calcium carbonate crystals.

There are two major forms of amoeboid cells in oyster hemolymph: agranulocytes and granulocytes (17–19). Agranulocytes tend to spread out thinly across a glass cover slip and secrete collagen fibers (20). Granulocytes are highly motile cells that appear to have a macrophage-like function (19). Some of these latter cells form a subclass known as

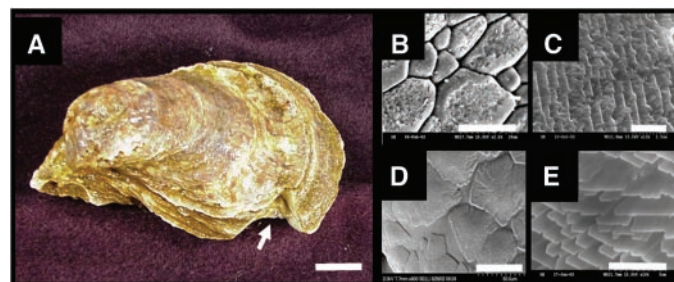
refractive granulocytes (REF granulocytes or REF cells), which contains the birefringent granules (fig. S1). REF granulocytes have been reported to be spent granulocytes (21), whereas others consider them to be the result of cellular differentiation, thus opening the possibility that they may have some role in shell formation (19, 22).

In order to observe cellular involvement in shell formation, we induced rapid shell growth by notching the oyster in the shell margin where the highest rates of biomineralization are observed (23). Newly formed shell is observed as a light brown to dark purple leather-like material that is lightly mineralized (24). Figure 1A is an image of an intact oyster, 48 hours after induction. Regenerated shell, indicated by the arrow, is visible within the notched region of the shell.

There are three distinct shell layers associated with an adult oyster shell. The outermost layer, or periostracum, is composed chiefly of organic matrix, which has a smooth appearance when examined by SEM (23–25). Immediately below the periostracum is the prismatic layer of the shell. It is a thin sheet of calcite composed of crystals in the form of prisms surrounded by organic matrix (Fig. 1, B and D) (24). The innermost foliated layer covers the underlying prismatic layer of shell and constitutes most of the mineralized shell volume (Fig. 1C). It is composed of layers of thin laths of calcite.

A common criticism of shell induction experiments is that the shell layers of regenerated shell do not resemble those associated with normal shell growth (15, 26). Our SEM observations of regenerated outer prismatic and inner foliated layers from notched oysters, however, do resemble their normal counterparts with some minor exceptions. Comparison of regenerated prismatic shell (Fig. 1D) to adult prismatic shell (Fig. 1B) shows newly formed prisms growing across the surface of the periostracum. These prisms have not yet completely covered the outer membrane but have the

Fig. 1. (A) Eastern Oyster *C. virginica* at 48 hours after induction. The arrow points to new shell that has regenerated within the cut or notched region of the mollusk. Bar, 1 cm. (B) SEM of mature prismatic shell. The prisms range from 5 to 25 μm in edge length. Bar, 20 μm . (C) Mature foliated shell showing individual laths that appear to be coated with organic material. Bar, 2.5 μm . (D) SEM of regenerated prismatic shell 48 hours after induction. The prisms are nearly the same size as in (B) yet have not completely grown together. Periostracum is visible as a smooth unmineralized sheet between the crystals. Bar, 50 μm . (E) Regenerated foliated shell 48 hours after induction. The individual laths appear free of debris and are arranged as in (C). Laths range from 0.25 to 5.3 μm in width (23). Bar, 5 μm .



¹Department of Biological Sciences, Clemson University, Clemson, SC 29634, USA. ²Center for Advanced Engineering Fibers and Films, Clemson University, Clemson, SC 29634, USA. ³1581 Regimental Lane, Johns Island, SC 29455, USA.

*To whom correspondence should be addressed. E-mail: mount@clemson.edu

†Present address: Dow Chemical Company, Analytical Sciences, 2301 North Brazosport Boulevard, Building B 1470, Freeport, TX 77541, USA.

same irregular shapes and sizes as in adult shell (Fig. 1B). A comparison of regenerated folia (Fig. 1E) to adult folia (Fig. 1C) reveals an identical microstructure of the crystals with the exception that newly formed folia have smoother surfaces and sharper edges than those of mature shell.

Several observations suggest that REF granulocytes play a role in the induced biomineralization response of oysters. First, comparisons of hemocytes collected at time of induction to those collected at 48 hours after induction indicate that there is an increase of REF granulocytes from 5 to 15% of the total hemocyte population (Table 1). Second, SEM of REF granulocytes reveal crystal-shaped inclusions in these cells (Fig. 2A; fig. S2). The edge length of the crystals ranged from 0.5 to 1 μm (Fig. 2B). It is likely that the inclusions are calcium carbonate crystals, given their rhombohedral appearance and the fact that line scan and spot analyses by x-ray microanalysis (SEM-EDS) confirmed that they contain calcium at higher levels than surrounding regions of the cell (Fig. 2B; fig. S3). Third, crystal-bearing REF granulocytes appear to release their crystals at the mineralization front. SEM observations of regenerated (newly formed) shell pieces revealed REF cells on the prismatic shell surface in association with lines of fibrous materials and crystals (Fig. 3A; fig. S4). Several of these cells are clustered in close association with secreted crystals (Fig. 3, A and B). Some cells contain just one or two crystals (Fig. 3C), whereas others contain several (Fig. 3D; fig. S5). In Fig. 3D, crystals in varying stages of cellular release are evident. These observations of directed activity at the mineralization front suggest that the REF granulocytes represent a developmental stage that delivers crystals to the site of shell formation.

Further evidence that living hemocytes are present at the mineralization front was obtained using the vital fluorescent stain, calcein AM. Hemocytes can be observed (Fig. 4) on newly regenerated prismatic shell. The labeled cells ranged in size from 14 to 20 μm .

Table 1. Hemocyte morphology at the time of induction (0 hours) and 48 hours after induction of shell in *C. virginica*. Data were normalized to percent from a mean of three different oysters. A minimum of five fields from each oyster's hemolymph sample was enumerated.

Hemocyte morphology	Percent	
	0 hours	48 hours
Agranulocytes	55	54
Non-REF granulocytes	40	31
REF granulocytes	5	15
Total	100	100

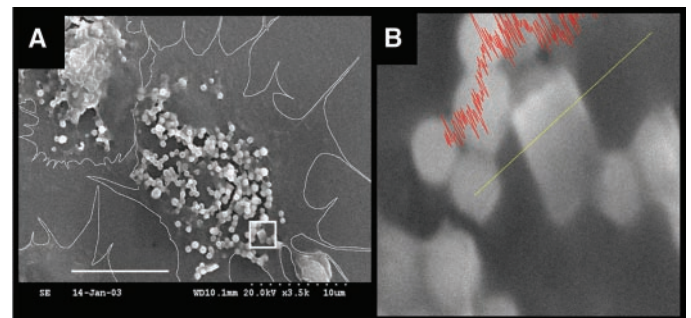
One cell had filopodia-like extensions around its periphery (Fig. 4A), whereas the other appeared more elongated with pseudopod-like projections (Fig. 4B), resembling the cell in Fig. 3D. Both cells appeared motile and shared the same morphological features as circulating oyster hemocytes.

Crystals released at the regeneration front have a striking appearance in that their morphology resembles inorganic calcite and their surfaces appear clean with sharply defined edges. However, they are quickly remodeled. Crystals presumably secreted by hemocytes at the margin of the newly formed shell are depicted in Fig. 3E. The crystals have grown in size, and holes can be seen near the centers of several individual crystals. They appear to be dissolved by a process that starts near their

centers and terminates when only the outer walls remain (Fig. 3F). A single remodeled crystal may yield several plates, all of uniform thickness and with dimensions similar to those of the foliated laths of regenerated shell (Fig. 1E). Preliminary indications are that hemocytes actively participate in these remodeling and assembly processes.

The supply of crystalline calcium carbonate by hemocytes can occur at a rate sufficient to support normal shell formation in oysters. Radioisotope incorporation studies estimate an average of 6 μg per cm^2 of mantle per hour calcium deposited in oysters as shell (2, 14, 27). Based on the average crystal size of secreted crystals detected by SEM (Fig. 3) and assuming four crystals are secreted per cell, it is estimated that 200,000

Fig. 2. SEM of crystal-bearing REF granulocytes isolated from hemolymph, 48 hours after induction. (A) The peripheries of four cells are outlined in white. The membrane has been removed from the largest cell, revealing many cytoplasmic granules and the presence of a single crystal in the cell. The box highlights the crystal within the cell. Bar, 10 μm . (B) Enlargement of the box in (A). The polyhedral shape resembles a calcite crystal. The crystal was subjected to SEM-EDS by line scan. The scanned region is indicated by the straight line. The jagged line shows count intensity obtained from the calcium main alpha K line. Bar, 1 μm . The crystal contains a higher relative abundance of calcium in comparison to the cellular background, including the spherical cytoplasmic granule that was scanned to its left (23).



The box highlights the crystal within the cell. Bar, 10 μm . (B) Enlargement of the box in (A). The polyhedral shape resembles a calcite crystal. The crystal was subjected to SEM-EDS by line scan. The scanned region is indicated by the straight line. The jagged line shows count intensity obtained from the calcium main alpha K line. Bar, 1 μm . The crystal contains a higher relative abundance of calcium in comparison to the cellular background, including the spherical cytoplasmic granule that was scanned to its left (23).

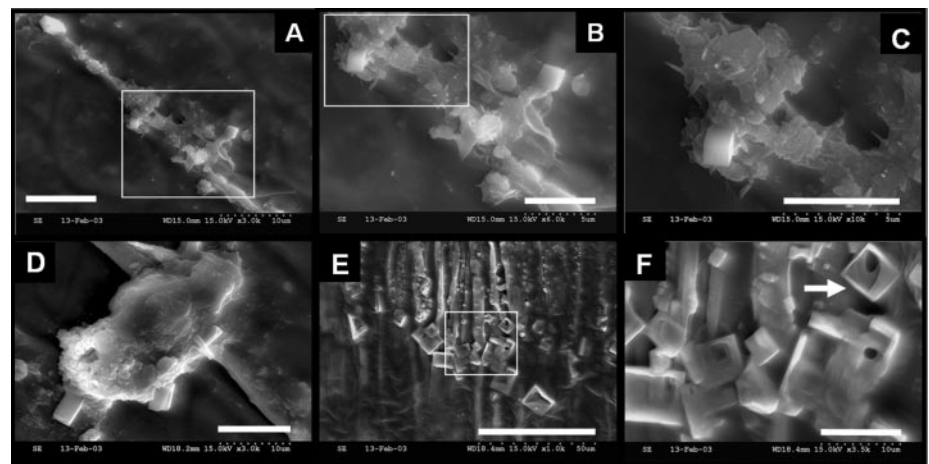


Fig. 3. (A) SEM of crystal-bearing hemocytes (REF granulocytes) of newly formed prismatic shell on the mineralization front, 48 hours after induction. The cells are oriented along a line of filamentous secretions and at least three crystals are visible. Bar, 10 μm . (B) Enlargement of the box in (A). Two crystals associated with two different hemocytes are visible. Bar, 5 μm . (C) Enlargement of the box in (B). A single crystal-bearing hemocyte is visible and the crystal size is 2 μm by 2 μm . Bar, 5 μm . (D) Crystal-bearing hemocyte disgorging several crystals at once. Crystal sizes range from 1 μm by 2 μm to 2 μm by 4 μm edge length. The crystals have a polyhedral shape that resembles calcite. Bar, 10 μm . (E) Crystals that appear to be undergoing remodeling. These crystals occur in the transition between prismatic and foliated shell layers. Bar, 50 μm . (F) Enlargement of the box in (E). The walls of the dissolved crystals have formed plate-like structures with dimensions more similar to foliated laths (arrow) (23). Bar, 10 μm .

REF cells would be required to sustain this level of mineralization. Typical *C. virginica* hemocyte counts averaged approximately 10 million cells per ml, which falls within the range of published values (18, 28). Assuming conservatively that an oyster has about 3 ml of hemolymph and that during periods of active shell growth 10% of the hemal cell population is crystal-bearing REF granulocytes (Table 1), then only approximately 7% of the REF cell population would need to be

regenerated per hour to sustain the reported average rate of calcium incorporation into shell. In addition, intracellular deposits of calcite in REF granulocytes could account for the large (approximately 97%) nonexchangeable pool of bivalve mantle tissue calcium that has been reported in several radioisotope studies (13, 14, 29).

A separate class of calcium carbonate crystals has been observed on the shell-forming surface of the OME (Fig. 5A).

Fig. 4. Fluorescent microscopy of living cells on a regenerated prismatic shell piece, 48 hours after induction. Shell pieces are incubated in calcein AM, a fluorescent reagent that determines cell viability. The esterase activity of living cells cleaves the dye, producing a charged green fluorescent product (23). The organic matrix that forms the walls of the prisms is autofluorescent in the FITC (fluorescein isothiocyanate) channel and is visible in the background. (A) Granulocyte exhibiting filopodia-like extensions around its periphery. Esterase-positive granules can be seen. Bar, 10 μm . (B) Calcein-positive hemocyte that resembles the cell in Fig. 3D. Several pseudopodia are visible. Bar, 10 μm .

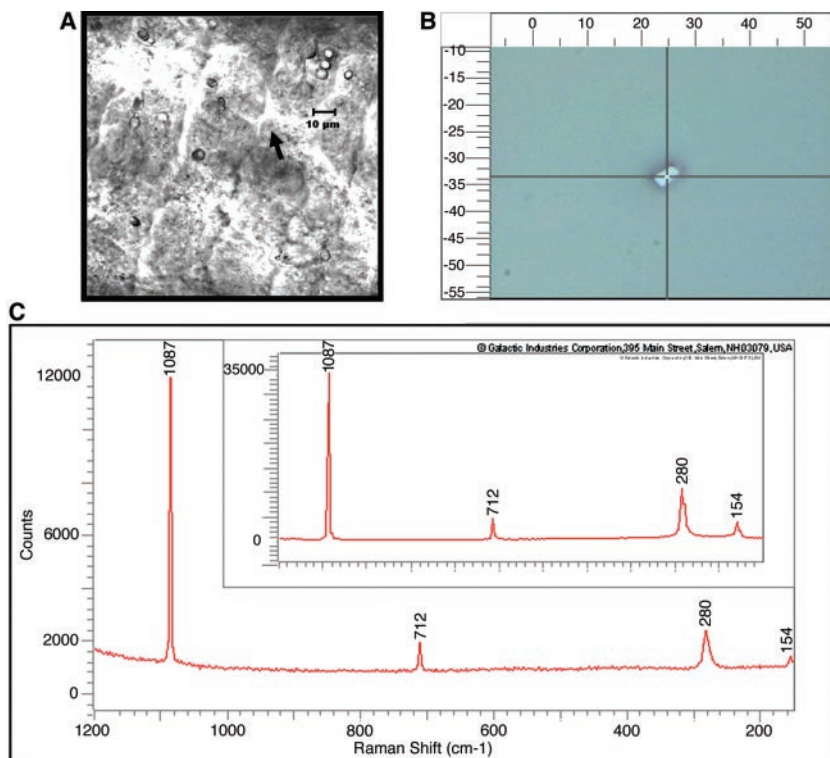
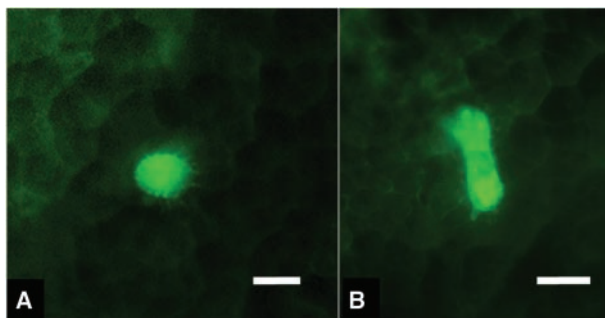


Fig. 5. (A) DIC (differential interference contrast) light micrograph of shell facing (OME) with cell junctions clearly visible, as indicated by the arrow. Note the individual crystals (in the upper right corner of the panel), which have edge lengths of approximately 5 to 7 μm . Bar, 10 μm . (B) Extracted crystal from the surface of the OME, shown in the crosshairs of the Raman confocal microscope, before excitation with the laser. (C) Raman spectra of the crystal showing peak intensities at 1087, 712, 280, and 154 cm^{-1} Raman shift. The inset figure is a calcite standard that has the same peak intensities. From these data it was concluded that the crystals on the shell-facing surface of the OME are calcite crystals, consistent with the mineralogy of both prismatic and foliated shell layers (23).

Although the general OME is not as active as the gland located in the periostracal groove (25, 30), it is involved in shell thickening and its surface is accessible to hemocytes (16, 17). Raman microspectroscopy of OME-extracted crystals revealed their mineralogy to be calcite, consistent with the known mineralogy of prismatic and foliated shell layers (23) (Fig. 5C). Although OME crystals have similar appearances and shapes as crystals released by hemocytes, they are somewhat larger in size (5 to 7 μm edge length) than the newly secreted crystals (1 to 4 μm edge length) (Fig. 5, A and B). We speculate that the OME-deposited crystals arise from nascent crystal secretions of REF cells and grow after deposition onto the surface of the OME.

A cellular basis for oyster shell formation is consistent with many other biomineralization processes, such as spicule formation. Spicules occur in most phyla, including notably the Mollusca (3, 31). In most of these taxa, spicule mineralization is usually mediated by a single cell type (scleroblast) and involves filamentous collagen-like proteins, and mature spicules form extracellular structures that may undergo further growth and remodeling.

The involvement of cells in shell formation may have evolutionary significance for the Mollusca. Scheltema's phylogeny of extant Mollusca proposes two separate evolutionary lineages: Aculifera (spicule formers) and Conchifera (shell formers) (32, 33). Although any cellular processes of mineralization in the two groups may be strictly homologous, it is possible that they have a common origin.

The discovery that hemocytes can initiate mineral growth on secreted organic sheets reduces the difficulties associated with nucleation of crystals from oyster extrapallial fluid, which at best is marginally supersaturated (10, 11). Apparently, crystal formation involves complex interactions between organic phases and cells.

References and Notes

1. K. Simkiss, K. M. Wilbur, *Biomineralization, Cell Biology and Mineral Deposition* (Academic Press, New York, 1989).
2. A. P. Wheeler, in *Calcification in Biological Systems*, E. Bonucci, Ed. (CRC Press, Boca Raton, FL, 1992), pp. 179–216.
3. H. A. Lowenstam, S. Weiner, *On Biomineralization* (Oxford Univ. Press, Oxford, 1989), pp. 74–175.
4. J. Aizenberg, D. A. Muller, J. L. Grazul, D. R. Hamann, *Science* **299**, 1205 (2003).
5. A. M. Belcher et al., *Nature* **381**, 56 (1996).
6. S. Mann, B. R. Heywood, S. Rajam, J. D. Birchall, *Nature* **334**, 692 (1988).
7. G. S. Falini, S. Albeck, S. Wiener, L. Addadi, *Science* **271**, 67 (1996).
8. L. A. Addadi, J. Moradian, E. Shay, N. G. Maroudes, S. Weiner, *Proc. Natl. Acad. Sci. U.S.A.* **84**, 2732 (1987).
9. E. M. Greenfield, D. C. Wilson, M. A. Crenshaw, *Am. Zool.* **24**, 925 (1984).
10. M. A. Crenshaw, *Biol. Bull.* **143**, 506 (1972).
11. A. S. Mount, thesis, Clemson University (1999).

12. C. S. Sikes, A. P. Wheeler, A. Wierzbicki, A. S. Mount, R. A. Dillaman, *Biol. Bull.* **198**, 50 (2000).
 13. L. H. Jodrey, *Biol. Bull.* **104**, 398 (1953).
 14. K. M. Wilbur, L. H. Jodrey, *Biol. Bull.* **103**, 269 (1952).
 15. K. M. Wilbur, in *Physiology of Mollusca*, K. M. Wilbur, C. M. Yonge, Eds. (Academic Press, New York, 1964), vol. 1, pp. 242–282.
 16. A. F. Eble, in *The Eastern Oyster, Crassostrea virginica*, V. S. Kennedy, R. I. E. Newell, A. F. Eble, Eds. (Maryland Sea Grant College, College Park, MD, 1996), pp. 271–298.
 17. T. C. Cheng, in *Invertebrate Blood Cells*, N. A. Ratcliffe, A. F. Rowley, Eds. (Academic Press, London, 1981), pp. 233–300.
 18. E. Gosling, *Bivalve Molluscs, Biology, Ecology and Culture* (Blackwell Publishing, Oxford, 2003).
 19. T. C. Cheng, in *The Eastern Oyster, Crassostrea virginica*, V. S. Kennedy, R. I. E. Newell, A. F. Eble, Eds. (Maryland Sea Grant College, College Park, MD, 1996), pp. 299–333.
 20. M. Justus, S. Patel, A. S. Mount, poster presented at the 6th International Conference on Shellfish Restoration, Charleston, SC, 20 to 24 November 2002.
 21. M. G. McCormick-Ray, T. Howard, *J. Invertebr. Pathol.* **58**, 219 (1991).
 22. P. M. Hine, *Fish Shellfish Immunol.* **9**, 367 (1999).
 23. Materials and methods are available as supporting material on Science Online.
 24. M. R. Carrier, R. E. Palmer, R. S. Prezant, *Proc. Natl. Shellfish Assoc.* **70**, 139 (1980).
 25. M. R. Carrier, in *The Eastern Oyster, Crassostrea virginica*, V. S. Kennedy, R. I. E. Newell, A. F. Eble, Eds. (Maryland Sea Grant College, College Park, MD, 1996), pp. 75–167.
 26. P. S. Galtsoff, *Fish Bull.* **64**, 1 (1964).
 27. K. M. Wilbur, A. S. M. Saleuddin, in *The Mollusca*, K. M. Wilbur, Ed. (Academic Press, New York, 1983), vol. 4, part 1, pp. 236–288.
 28. S. E. Ford, S. A. Kanaley, D. T. Littlewood, *J. Invertebr. Pathol.* **61**, 49 (1993).
 29. A. P. Wheeler, P. L. Blackwelder, K. M. Wilbur, *Biol. Bull.* **148**, 472 (1975).

30. N. Watabe, in *The Mollusca*, K. M. Wilbur, Ed. (Academic Press, New York, 1983), vol. 4, part 1, pp. 289–317.
 31. R. J. Kingsley, *Am. Zool.* **24**, 833 (1984).
 32. A. H. Scheltema, *Biol. Bull.* **184**, 57 (1993).
 33. A. H. Scheltema, C. Schander, *Biol. Bull.* **198**, 121 (2000).
 34. We thank E. Ruppert, R. Montanucci, and D. Bushek for careful reading and suggestions that have improved the quality of this manuscript. We also thank J. Hatchell for his efforts in cell enumeration and construction of the oyster holding facility; B. Kay for technical help with EM; J. Mount for assistance in revised figure preparation; and T. McNutt Scott, M. Johnstone, S. Patel, and M. Justus for invaluable discussions. We gratefully acknowledge support from NSF under award no. 20020445.

Supporting Online Material
www.sciencemag.org/cgi/content/full/304/5668/297/DC1
 Materials and Methods
 Figs. S1 to S5
 References

15 August 2003; accepted 2 March 2004

Characterization of a Common Susceptibility Locus for Asthma-Related Traits

Tarja Laitinen,^{1,2} Anne Polvi,² Pia Rydman,¹ Johanna Vendelin,^{1,2} Ville Pulkkinen,¹ Paula Salmikangas,¹ Siru Mäkelä,² Marko Rehn,¹ Asta Pirskanen,¹ Anna Rautanen,⁴ Marco Zucchelli,⁵ Harriet Gullstén,^{2,5} Marina Leino,⁶ Harri Alenius,⁶ Tuula Petäys,⁷ Tari Haahela,⁷ Annika Laitinen,³ Catherine Laprise,⁹ Thomas J. Hudson,¹⁰ Lauri A. Laitinen,⁸ Juha Kere^{*2,5}

Susceptibility to asthma depends on variation at an unknown number of genetic loci. To identify susceptibility genes on chromosome 7p, we adopted a hierarchical genotyping design, leading to the identification of a 133-kilobase risk-conferring segment containing two genes. One of these coded for an orphan G protein-coupled receptor named GPRA (G protein-coupled receptor for asthma susceptibility), which showed distinct distribution of protein isoforms between bronchial biopsies from healthy and asthmatic individuals. In three cohorts from Finland and Canada, single nucleotide polymorphism-tagged haplotypes associated with high serum immunoglobulin E or asthma. The murine ortholog of GPRA was up-regulated in a mouse model of ovalbumin-induced inflammation. Together, these data implicate GPRA in the pathogenesis of atopy and asthma.

Asthma is a complex phenotype with a proven genetic component, and several projects to map susceptibility genes for asthma and re-

lated traits have been undertaken (1). The first published genome-wide scan in asthma suggested six tentative genetic loci, among them chromosome 7p, which was then strongly implicated in a study of Finnish and Canadian families and confirmed in West Australian families (2–4). To positionally clone asthma candidate genes on chromosome 7p, we studied the Finnish Kainuu subpopulation and considered three alternative hypotheses. First, that only one copy of the susceptibility allele may have survived in this population, with long-conserved haplotypes being observed, as would be consistent with some previous findings (5–7). Second, there might exist a founder effect, common to many European populations. This would be consistent with the common disease/common variant hypothesis, as observed for example

in psoriasis (8, 9). In this case, the carrier frequency should be higher than a few percent, with only a short conserved haplotype (<200 kb) detected (8). Third, numerous mutations might exist in the putative gene, in which case only weak or absent haplotype associations might be detectable.

To distinguish between these hypotheses, we adopted a genotyping scheme whereby we increased the density of markers used, with intermediate analyses to guide further genotyping (Fig. 1A). More specifically, if genetic association analysis suggested that a haplotype occurred in patients more often than in controls, additional markers were genotyped to either exclude or support the identity-by-descent of the haplotypes observed in unrelated patients. For the haplotypes to be identical by descent, all newly typed markers would have to be identically shared between them. The genotyping was done on 86 original genome scan families and an additional 103 trios (all together, 874 subjects) (10). Successive rounds of genotyping and analysis by the haplotype pattern mining (HPM) algorithm (11) suggested the strong association of a conserved haplotype pattern spanning between NM51 and SNP563704, separated by 46 kb (Fig. 1A). The HPM algorithm searches for allele patterns shared between several haplotypes among large sets of unrelated haplotypes.

To fully explore the genetic variation in associated haplotypes, we sequenced nonrepetitive DNA segments in this interval (from position 506,401 to 638,799 in the public sequence NT_000380; all positions are given with reference to this sequence) in one patient homozygous for the susceptibility haplotype and one control subject homozygous for the most common (nonrisk) haplotype. These sequences were then compared to the public sequence (NT_000380). Two observations emerged from these analyses: first, the patient did not reveal a single instance of heterozygosity, confirming the identity-by-descent of this chromosome segment. Second, comparison of the susceptibility

¹GeneOS Limited, 00251 Helsinki, Finland. ²Department of Medical Genetics, ³Department of Anatomy, Biomedicum Helsinki, University of Helsinki, 00014 Helsinki, Finland. ⁴Finnish Genome Center, University of Helsinki, 00014 Helsinki, Finland. ⁵Department of Biosciences at Novum and Clinical Research Centre, Karolinska Institutet, 14157 Huddinge, Sweden. ⁶Department of Industrial Hygiene and Toxicology, Finnish Institute of Occupational Health, 00251 Helsinki, Finland. ⁷Department of Allergological Diseases, ⁸Department of Medicine, Helsinki University Central Hospital, 00029 Helsinki, Finland. ⁹Community Genomic Medicine Centre, Université du Québec à Chicoutimi, Saguenay, Quebec G7H 2B1 Canada. ¹⁰McGill University and Genome Quebec Innovation Centre, Montreal, Quebec H3A 1A4 Canada.

*To whom correspondence should be addressed. E-mail: juha.kere@biosci.ki.se



Hemocyte-Mediated Shell Mineralization in the Eastern Oyster

Andrew S. Mount *et al.*
Science **304**, 297 (2004);
DOI: 10.1126/science.1090506

This copy is for your personal, non-commercial use only.

If you wish to distribute this article to others, you can order high-quality copies for your colleagues, clients, or customers by [clicking here](#).

Permission to republish or repurpose articles or portions of articles can be obtained by following the guidelines [here](#).

The following resources related to this article are available online at www.sciencemag.org (this information is current as of March 5, 2016):

Updated information and services, including high-resolution figures, can be found in the online version of this article at:

</content/304/5668/297.full.html>

Supporting Online Material can be found at:

</content/suppl/2004/04/07/304.5668.297.DC1.html>

A list of selected additional articles on the Science Web sites **related to this article** can be found at:

</content/304/5668/297.full.html#related>

This article **cites 22 articles**, 11 of which can be accessed free:

</content/304/5668/297.full.html#ref-list-1>

This article has been **cited by** 61 article(s) on the ISI Web of Science

This article has been **cited by** 12 articles hosted by HighWire Press; see:

</content/304/5668/297.full.html#related-urls>

This article appears in the following **subject collections**:

Biochemistry

</cgi/collection/biochem>